Advanced SLMs for Microscopy

A. Linnenberger
Meadowlark Optics, 5964 Iris Parkway, Frederick, CO, USA 80530

ABSTRACT

Wavefront shaping devices such as deformable mirrors, liquid crystal spatial light modulators (SLMs), and active lenses are of considerable interest in microscopy for aberration correction, volumetric imaging, and programmable excitation. Liquid crystal SLMs are high resolution phase modulators capable of creating complex phase profiles to reshape or redirect light within a three-dimensional (3D) volume. Recent advances in Meadowlark Optics (MLO) SLMs reduce losses by increasing fill factor from 83.4% to 96%,and improving resolution from 512 x 512 pixels to 1920 x 1152 pixels while maintaining a liquid crystal response time of 300 Hz at 1064 nm. This paper summarizes new SLM capabilities, and benefits for microscopy.

Keywords: high speed, high resolution, low loss, spatial light modulator, liquid crystal on silicon, LCOS, SLM

1. INTRODUCTION

Microscopy is a critical field for much of biology and medicine, resulting in a substantial scope of applications requiring wavefront control. This paper will focus on neuroscience because of the impact the Brain Research through Advancing Innovative Neurotechnologies (BRAIN) initiative has had in uniting researchers from the fields of Chemical Engineering, Electrical Engineering, Physics, and Neuroscience in the common goal of understanding the human brain. This effort is driven by a lack of understanding of neurological disease, and a lack of quantitative measures to assess how therapeutics impact brain functions. The problem represents a significant healthcare cost today with projections that are unsustainable. The Alzheimer's Association reports that in 2013 Alzheimer's cost the nation $203 billion, and is projected to cost $1.2 trillion by 2050 [1]. Progress necessitates the development of new tools to understand how neural circuits function such that more effective and localized treatments can be developed, and quantitative measurements of how therapeutics act on neural circuits can be established.

In the last decade, neuroscientists have begun to transition from traditional tools for neuroscience, including electrical recordings of cellular activity using a patch clamp and imaging voxels containing millions of neurons using the fMRI, to a new set of optical techniques. These techniques use light to monitor and manipulate the activity of neuronal ensembles with single cell resolution, *in vitro* and *in vivo*. The combination of optical methods with genetically encoded photosensitive proteins (referred to as *optogenetics*) and optochemical (caged) compounds now offers the opportunity to image the activity of many neurons through calcium imaging and optically control them through photostimulation.

In calcium imaging, cells are loaded with chemical indicators that bind with calcium during an action potential. If the cell is illuminated with an excitation source during the action potential, then there is a localized fluorescence spike. In photostimulation, tissue is loaded with compounds that cleave when illuminated, stimulating receptors in neighboring cells causing an action potential. These techniques are fast, enabling researchers to monitor and manipulate cellular activity on timescales approaching 1 kHz [2] and can be used on large numbers of cells with a spatial specificity of less than 1 μm [3]. Light is less invasive than electrodes and offers considerable flexibility and simple multisite modulation. Finally, optical techniques can have single cell resolution, while retaining the ability to target a large number of cells within a volume of the brain. This is critical for understanding the function of neural circuits, and how that function is altered by disease.

Confocal microscopes have become an essential tool for microscopy. However, the need to monitor and manipulate firing patterns of neural circuits in a 3D volume has driven the development of advanced two photon microscopes for neuroscience. Scanning two photon microscopes use resonant stages, galvanometer scanners, or fast random-access serial scanning using acousto-optic deflectors to raster scan a laser through the sample to build an image pixel by pixel. This can result in scanning rates of 50 kHz. However, it is still difficult to achieve simultaneous multisite stimulation with this approach because it is necessary for the laser to dwell at each location to collect enough photons to generate a usable image or to modulate the activity. Attempts to circumvent this by increasing the peak excitation intensity are fundamentally limited, because the high intensity triggers photo-damage of the neurons and photo-bleaching of the

A. Linnenberger, "Advanced SLMs for Microscopy", Proc. SPIE 10502, Adaptive Optics and Wavefront Control for Biological Systems IV, 1050201 (23 February 2018); doi: 10.1117/12.2290455; https://doi.org/10.117/12.2290455

fluorophores. Furthermore, traditional microscopes are limited to imaging two-dimensional surfaces, while neural circuits have three-dimensional structure. Depth scanning can be used to build a 3D image but is very slow as it is typically realized by scanning the objective at rates of around 20 Hz. This is insufficient to monitor neural activity which occurs on the timescale of a single millisecond. As a result, one only images a small subset of the neurons, and therefore collects a limited picture of the total activity. For optogenetics research, there is a need for a microscope capable of dynamic and arbitrary formation of multiple foci in 3D to monitor and manipulate firing patterns, and the microscope must be capable of 3D imaging in order to capture the response of the circuit.

Adding a liquid crystal spatial light modulator in the excitation path of a scanning two-photon microscope allows the excitation source to be divided to create hundreds of independent foci, and to reconfigure the 3D position of the foci at rates of up to 300 Hz. Thus, using SLMs one can deliver light to simultaneously excite multiple 3D sites to first stimulate activity, and then to target cells in a volume to monitor the response of the neural circuit to the stimulation. This parallelizes the process of monitoring and manipulating activity of neurons among a large population of cells. The potential for use of SLMs in optogenetics was first demonstrated by Yuste *et al* with the development of a prototype SLM based microscope that allows for the simultaneous excitation of multiple neurons in brain slices [4]. In that work, Yuste simultaneously imaged and detected action potentials in dozens of neurons, with frame rates of 66 Hz. This was a significant advancement for the neuroscience community, but the work was limited by the SLMs available to Yuste at the time. This work has driven development of advanced SLMs to improve resolution to maximize the volume of the brain that can be studied, to improve power handling to increase the number of neurons that can be illuminated at a time, and to improve response time such that the excitation can match neural circuit dynamics.

2. LATERAL EXCITATION

In order for the SLM to excite a volume of neurons, it is not sufficient to use the SLM as an amplitude modulator that is imaged to the sample. Instead, the SLM must be used as a phase modulator, and a hologram that is the Fourier transform of the desired excitation pattern is written to the SLM. Using an optical relay, the SLM is imaged to the back focal plane of the objective. To utilize the full numerical aperture (NA) of the objective, and thus not sacrifice the confinement of excitation, the image of the SLM at the objective should fill the back aperture. The size of the pixel pitch in the image of the SLM at the objective, referred to as the *effective pixel pitch*, is dependent on the relay optics (Figure. 1). The lateral field of view of excitation is driven by the smallest phase grating that can be written to the SLM. From the grating equation $\sin(\theta) = m*\lambda/d$, one can compute the widest angle that light can be steered to. This is dependent on the order m which is set to one, the wavelength λ, and the period of the grating d which at a minimum is 2x the effective pixel pitch. Beamsteering angle is converted to lateral displacement at the sample by the focal length of the objective.

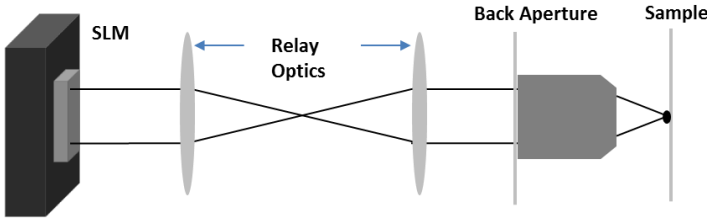

Figure 1. The SLMs is imaged to the back focal plane of the objective such that the image of the SLM fills the back focal plane, and by applying holograms to the SLM focal points or regions of interest are created at the sample.

For this analysis, a binary 0, π grating is considered as this is the theoretical limit of lateral excitation imposed by the physical structure of the backplane. The practical limit will depend on the laser power available, and minimum 1st order intensity required for excitation. First order diffraction efficiency is quantified by the ratio of light in the 1st order when writing a repeating phase ramp to the SLM as compared to 0th order intensity when writing a blank pattern to the SLM. Figure 2 summarizes 1st order diffraction efficiency of the 1920 x 1152 pixel SLM at 1064 nm for a phase ramp consisting of 32 pixels, 16 pixels, 8 pixels, and 4 pixels.

A. Linnenberger, "Advanced SLMs for Microscopy", Proc. SPIE 10502, Adaptive Optics and Wavefront Control for Biological Systems IV, 1050201 (23 February 2018); doi: 10.1117/12.2290455; https://doi.org/10.117/12.2290455

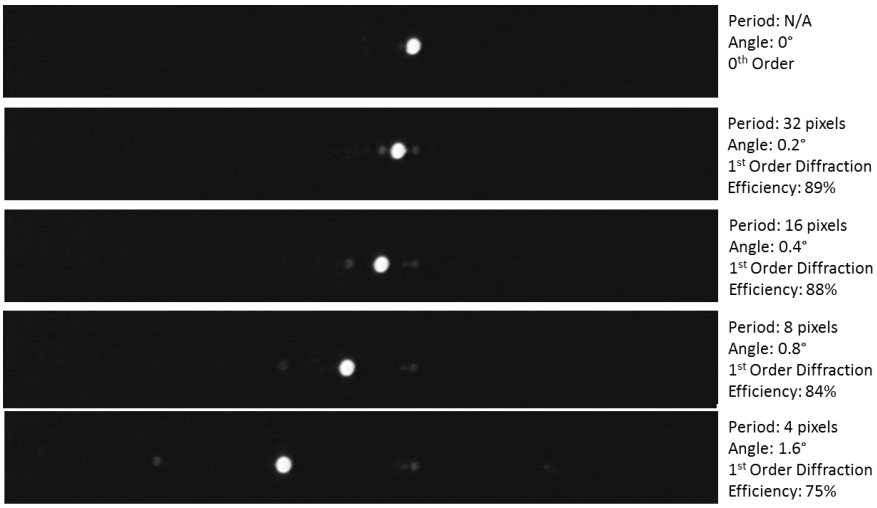

Figure 2 First order diffraction efficiency as a function of beamsteering angle for the high speed 1920 x 1152 pixel SLM at 1064 nm.

Much research in optogenetics has utilized the MLO 512 x 512 pixel SLM because the maximum frame rate is 300 Hz at 1064 nm. However, the limited resolution of the SLM leaves a trade in field of view, and excitation confinement. For example, with a 25x 0.45 NA objective with a back aperture of 9.2 mm (Olympus XLPlan N), the image of the SLM must be magnified in the relay optics in order to fill the back aperture with the image of the SLM and thus utilize the full NA of the objective. This magnification increases the effective pixel pitch from 15 µm at the SLM to 18 µm in the image of the SLM at the back focal plane of the objective. The maximum angle that the SLM can steer to is realized when a binary 0, π grating with period of 2 pixels is written to the SLM. If the excitation wavelength is 940 nm, as is commonly utilized with GCaMP6, then the maximum angle that the SLM can steer to is 1.52°. The focal length of this objective is 7.2 mm, giving a maximum lateral displacement of ±188 µm about the 0^{th} order, or a total lateral displacement in x and y of 376 µm.

The choice to magnify the image of the SLM in the relay optics increased the disparity between the maximum lateral displacement of excitation that the SLM can steer to, which is ±188 µm, and the area that the objective can image, which is 720 µm. However, the magnification in the relay optics matches the image of the SLM to the dimensions of the back aperture of the objective, meaning that the full NA of the objective is utilized to create focal points for excitation. If the SLM is relayed with a demagnification such that the effective pixel pitch is 9.4 µm, then the maximum lateral displacement of excitation of the SLM can match the field of view that the objective can image. But, in this case the image of the SLM at the objective is 4.81 mm, and the back aperture is 9.2 mm, reducing the effective NA for excitation to 52% of the full NA. Thus, this design choice to match beamsteering of the SLM to field of view comes at the expense of lateral and axial confinement of excitation.

The lack of resolution in the SLM also limits the number of locations where focal points can be placed in the sample. Via the Fourier Transform, if the resolution of the SLM is 512 x 512 pixels is possible to produce 512 x 512 focal points in a 2D plane in the sample if the 0^{th} order is placed in the middle of the field of view. The objective used has a field of view of 720 µm. With a diffraction limited focal point waist of 0.537 µm, the objective is capable of generating 1340 x 1340 resolvable spots. Thus, the limitations in the number of available pixels at the SLM results in an under-utilization of the objectives resolvable focal points by a factor of 2.6 both in x and y.

By improving the resolution of the SLM from 512 x 512 to 1920 x 1152 pixels the trade between excitation confinement and field of view is removed. For optogenetics it is desirable to maintain the point spread function (PSF) of excitation in x and y, so a square region of interest of the SLM is imaged to the back focal plane of the objective, effectively reducing the SLM resolution to 1152 x 1152 pixels. The pixel-pitch of the SLM is 9.2 um, making the short axis of the SLM 10.6 mm. In order to match the dimensions of the image of the SLM to the back aperture of the objective, the relay optics must de-magnify the image of the SLM, reducing the effective pixel pitch to 8 µm. Taking the maximum grating frequency to be 2 pixels in a 0, π diffraction pattern, and taking the incident wavelength to be 940 nm, the maximum angle that the SLM can steer to is 3.36°. Taking the objective focal length to be 7.2 mm, the maximum lateral displacement is ± 423 µm about the 0^{th} order, or a total lateral displacement in x and y of 847 µm. This exceeds

the field of view that the objective can image while maintaining the full NA of the objective, and thus not sacrificing excitation confinement. Furthermore, via the Fourier Transform one can now create 1152 x 1152 focal points at the sample, which only under-utilizes the objectives resolvable focal points by a factor of 1.16.

Table 1 summarizes the objective specifications, optical system, lateral beamsteering specifications for the 1920 x 1152 pixel SLM and the 512 x 512 pixel SLM with and without matching the image of the SLM to the dimensions of the objective back aperture, and the objective utilization. The analysis can be replicated for different SLM models using the equations outlined.

Objective Specifications:			
Tube length	180 mm		
Objective magnification	25x		
Numerical Aperture	1.05		
Objective Focal Length	7.2 mm		
Objective aperture diameter	9.2 mm		
FN	18		
Field of View	720 µm		
Resolvable Spots	1430 x 1430		
Optical System			
Number of pixels	512 x 512	512 x 512	1152 x 1152
Pixel pitch	15 µm	15 µm	9.2 µm
SLM Active area (short axis)	7.68 mm	7.68 mm	10.6 mm
Magnification To Objective	1.197	0.6266	0.868
Effective Pixel Pitch	18 µm	9.4 µm	8 µm
Effective Numerical Aperture	1.05	0.55	1.05
Wavelength GCaMP	940 nm	940 nm	940 nm
Lateral Displacement			
Beamsteering Angle: $\sin(\theta) = m*\lambda/d$	1.496	2.866	3.368
Lateral Displacement	±188	±360	±423
Total Lateral Displacement	376 µm	720 µm	847 µm
Objective Utilization			
SLM Resolvable Spots	512 x 512	512 x 512	1152 x 1152
Factor of Objective Utilization	2.6	2.6	1.16

Table 1. The SLM resolution coupled with the objective specifications, choice of relay optics, and wavelength determine the specifications for the lateral field of view over which the SLM can steer light. This table compares the 512 x 512 pixel SLM when matching the image of the SLM to the back aperture of the objective, when under-filling the image of the SLM on the objective to sacrifice excitation confinement to match the field of the view of beamsteering to the objective, and the 1920 x 1152 where a 1152 x 1152 pixel image is relayed to the objective. The high resolution SLM matches the beamsteering capabilities of the SLM to the field of view of the objective without sacrificing excitation confinement.

3. AXIAL EXCITATION

In additional to steering light laterally, the SLM can apply lens functions to the wavefront to steer focal points axially in the sample. There are two factors that determine the maximum axial displacement of a focal point from the designed focal length of the objective. For some applications the spherical aberrations introduced by focusing beyond the designed focal length of the objective could cause a practical upper limit to axial defocus. The SLM can correct for aberrations, but the required quality of the focal point PSF is application specific. The second limit is a physical limit of the SLM, which can be calculated as the strongest lens function that the SLM can generate without aliasing on the outermost Fresnel zone [5]. This is quantified by $F_{SLM}=d^2*N/\lambda$, where d is the effective pixel pitch of the image of the SLM at the objective, N is the resolution of the SLM, and λ is the wavelength. The SLM can add or subtract from the focal length objective, which is quantified using the compound thin lens equation $F = (F_{obj}*F_{SLM})/(F_{obj} + F_{SLM})$. As with the lateral FOV calculations, the incident wavelength is taken as 940 nm and specifications of the Olympus XLPlan N are used.

A. Linnenberger, "Advanced SLMs for Microscopy", Proc. SPIE 10502, Adaptive Optics and Wavefront Control for Biological Systems IV, 1050201 (23 February 2018); doi: 10.1117/12.2290455; https://doi.org/10.117/12.2290455

With the 512 x 512 pixel SLM the focal point can be steered ±282 µm about the design focal plane of the objective if the image of the SLM fills the back aperture of the objective (the effective pixel pitch is 18 µm). If the image of the SLM under-fills the objective such that the effective pixel pitch is 9.4 µm, and the full NA of the objective is not utilized, then the axial beamsteering can be extended to ±937 µm. With the 1920 x 1152 pixel SLM, if the image of the SLM fills the back aperture of the objective and the effective pixel pitch is 8.0 um, then the axial beamsteering is ±467 µm.

Table 2 summarizes the optical system, axial beamsteering specifications for the 1920 x 1152 pixel SLM and the 512 x 512 pixel SLM with and without matching the image of the SLM to the dimensions of the objective back aperture.

Optical System			
Number of pixels	512 x 512	512 x 512	1152 x 1152
Pixel pitch	15 µm	15 µm	9.2 µm
SLM Active area (short axis)	7.68 mm	7.68 mm	10.6 mm
Magnification To Objective	1.197	0.6266	0.868
Effective Pixel Pitch	18 µm	9.4 µm	8 µm
Effective NA	1.05	0.55	1.05
Wavelength GCaMP	940 nm	940 nm	940 nm
Axial Displacement			
SLM Focal Length: $F=(d\text{^}2\ N)/\lambda$	176.47 mm	48.12 mm	103.73 mm
Combined focal length: F = (Fslm*Fobj)/(Fslm + Fobj)	6.98 mm	6.26 mm	6.73 mm
Delta From Objective Focal Length	282.24 µm	937.13 µm	467.33 mm
Total Axial Excitation Displacement	564.47 µm	1874.26 µm	934.652 µm

Table 2. The SLM resolution coupled with the objective specifications, choice of relay optics, and wavelength determine the specifications for the maximum axial displacement of focal points from the objective design focal length. This table compares the 512 x 512 pixel SLM when matching the image of the SLM to the back aperture of the objective, when under-filling the image of the SLM on the objective, and the 1920 x 1152 where a 1152 x 1152 pixel image is relayed to the objective.

4. POWER HANDLING

As the field of view of excitation increases, more neurons and larger neural circuits can be studied. In order to illuminate multiple objects in the field of view, the SLM divides the incident illumination into multiple foci. As the number of foci increases, the power per focal point decreases. In order to increase the number of excitation targets, while maintaining enough power per target to excite fluorescence, power handling of the SLM becomes critical. Multiple factors impact power handling. Increasing the size of the SLM allows the illumination to be spread over a larger area, coatings can be optimized to limit absorption, and active and passive cooling systems can be used to mitigate thermal effects.

For optogenetics many researchers are using femtosecond pulsed lasers. The Coherent Monaco is a 1035 nm pulse laser with a programmable pulse width that can range from 300 femtoseconds (FWHM, sech^2 fit) to 10 picoseconds. It has maximum pulse energy of 40 uJ, and at a pulse repetition rate of 1 MHz, the laser can output 40 Watts average power. The output beam profile is Gaussian with an M^2 value of ~1.1. Compatibility of the 1920 x 1152 pixel SLM was tested by incrementing the incident power from 101 MW/cm^2 to 729 MW/cm^2, while measuring the backplane temperature and the 1st order diffraction efficiency when writing a series of diffraction patterns to the SLM (Figure 3). When using the passive cooling system, changes in modulation depth were observed due to the 22 °C increase in backplane temperature as the incident power increased. However, at the maximum incident power the modulation depth was still greater than one wave, allowing the ability to characterize the optical response based on temperature and use the on chip sensors as a closed loop system to maintain 1st order diffraction efficiency independent of incident power. Alternatively, an active cooling block can be added to the SLM to sustain an operating temperature below 40 °C such that a consistent modulation depth is maintained independent of the incident power.

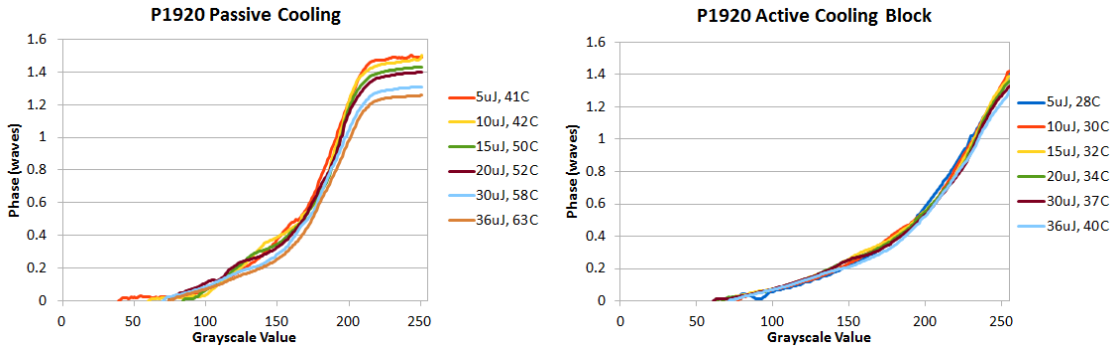

Figure 3. Modulation depth of a P1920 SLM as a function of pulsed laser average power, and SLM operating temperature. Laser parameters: 1MHz rep-rate, 280 fs pulse width, 6.7mm beam size ($1/e^2$). At the maximum energy output of 36uJ, 36W average power, average power density = 204W/cm^2, peak power = 128MW, peak power density = 729MW/cm^2. (left) modulation depth decreases as the incident power increases due to thermal effects of a passive cooling system (right) adding an active cooling system allows for consistent modulation depth at a peak power density of up to 729MW/cm^2.

5. RESPONSE TIME

Liquid crystal response time is dependent on multiple factors, including the thickness of the liquid crystal layer which is optimized to give one wave of phase stroke at the longest working wavelength, the voltage of the driver, and the liquid crystal material properties. For optogenetics most researchers are coupling SLMs with two-photon microscopes, and are working at wavelengths ranging from 700 nm to 1000 nm. MLO is the only SLM supplier to offer SLMs capable of switching from 0 – 2pi at 1064 nm at 300 Hz.

The method to achieve this switching speed is different based on the SLM model. The 512 x 512 pixel SLM is voltage limited, necessitating alternative drive schemes [6] to reach the desired frame rate, referred to as OverDrive Plus (ODP). This approach consists of two concepts. The first, referred to as the transient nematic effect, was first demonstrated by Wu [7]. As shown in Figure 4, if phase delay of a LC modulator is changed from ϕ_0 to ϕ_1, then the LC molecules relax into the new phase following approximately an exponential curve. In order to take advantage of the transient nematic effect, one instead changes the phase from ϕ_0 to ϕ_{max} to ϕ_1. This causes the relaxation to follow a different exponential curve until the desired phase is reached, resulting in a significantly improved switching speed.

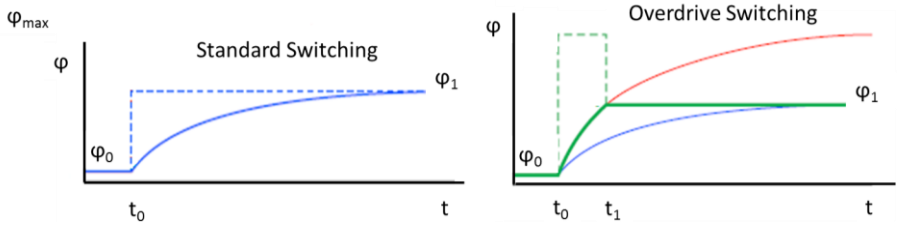

Figure. 4 (left) Standard switching, (right) ODP switching taking advantage of the transient nematic effect

The second concept incorporated into ODP is Phase Wrapping. Phase wrapping recognizes that ϕ_1 is equivalent to $\phi_1 + 2\pi$, and there are times when it is faster to transition from ϕ_0 to $\phi_1 + 2\pi$ as opposed ϕ_1. In order to realize this benefit it is necessary to regionally characterize the LC response to voltage such that the algorithm can compute the required intermediate voltage, how long to hold on that voltage, and what the ideal ending voltage should be to minimize response time. The solution to this problem was demonstrated by Thalhammer *et. al.* [6] when he demonstrated the ability to realize hologram switching speeds of 1 ms at 640 nm using the MLO 512 x 512 pixel SLM.

The challenge of Overdrive arises from the fact that when switching from one hologram to the next different pixels are at different voltages, and thus each pixel needs to switch to a specific intermediate voltage for a specific amount of time to benefit from the transient nematic effect. In order to accommodate this, a series of 6 to 10 transient images are computed and loaded in the transition between each user defined image. For applications requiring real time processing the transient images add significant computation overhead.

On the 1920 x 1152 pixel SLM, the backplane voltage combined with properties of the liquid crystal enable a 300 Hz frame rates at 1064 nm without requiring ODP, simplifying software and computational load. Figure 5 shows an

oscilloscope trace of a high speed 1920 x 1152 SLM translating a 1064 nm focal point translating on and off a point detector (yellow), an output pulse being generated by the hardware 1.18 ms prior to the new image loading to the SLM (purple), and image transfers driven by the falling edge of an external trigger (blue). The fast liquid crystal response time coupled with PCIe hardware to facilitate high speed image transfers and input and output triggers enable precise timing required to monitor and manipulate brain activity such that researchers can match excitation to temporal dynamics of neural circuits.

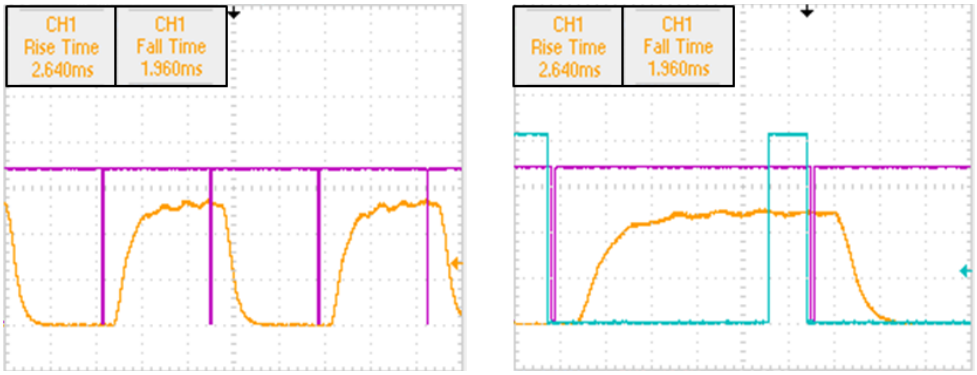

Figure. 5 The 10 to 90 rise and fall time of the liquid crystal switching a focal point on and off a detector in less than 3 ms at 1064 nm. (left) Liquid crystal switching driven by software timing. A focal point is toggled on and off a detector (shown in yellow). When the image on the SLM changes, the hardware can produce an output pulse (shown in purple) indicating a new image will begin loading on the SLM in 1.18 ms. (right) Liquid crystal switching driven by external hardware trigger. When the falling edge of an external trigger arrives (shown in blue) the hardware will initiate the update the image on the SLM. An output pulse is generated to acknowledge receipt of the trigger (shown in purple). The image will update on the SLM 1.18 ms after the output pulse was generated (shown in yellow with the focal point moving on and off the detector).

6. PHASE STABILITY

To ensure consistent excitation when the excitation source is divided among many neurons the temporal characteristics of the SLM become important. MLO SLMs use two strategies to maximize phase stability. The first strategy is use of direct analog addressing as opposed to simulation of analog modulation using binary addressing combined with time sequential dithering. The second strategy is use of custom backplanes capable of refreshing at a rate of 844 Hz. A high speed backplane refresh is necessary to mitigate the voltage loss from the capacitance of the pixel. If the backplane refresh is slow, then the voltage droop at the pixel allows the liquid crystal molecules to relax, changing the refractive index of the LC. If the backplane voltage is refreshed at a rate significantly faster than the LC relaxation time, then the SLM will have high phase stability.

Phase stability is quantified by writing a repeating phase ramp to the SLM, and measuring the 1st order intensity. Instabilities from the LC molecules relaxing will cause the intensity of the 1st order focal point to vary as a function of time. Phase stability is defined as the ratio of the peak to peak 1st order focal point intensity to the mean focal point intensity. For the 512 x 512 pixel SLM with ODP the phase ripple is 3% – 5%, and for the high speed 1920 x 1152 pixel SLM the phase ripple is 2% – 4% (Figure 6). For research requiring higher phase stability and high resolution the standard 1920 x 1152 pixel SLM offers a phase ripple as low as 0.20%.

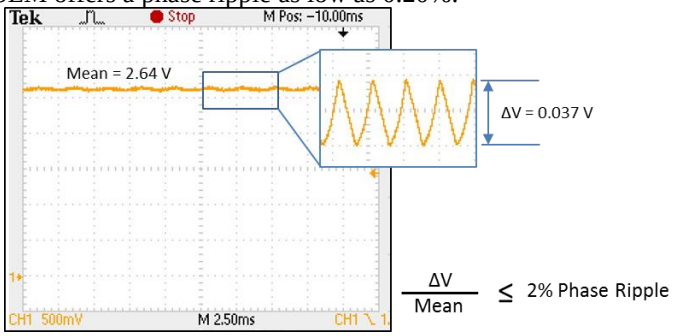

A. Linnenberger, "Advanced SLMs for Microscopy", Proc. SPIE 10502, Adaptive Optics and Wavefront Control for Biological Systems IV, 1050201 (23 February 2018); doi: 10.1117/12.2290455; https://doi.org/10.117/12.2290455

Figure. 6 Phase ripple of the high speed 1920 x 1152 pixel SLM. The mean first order intensity, and peak to peak first order intensity are measured when writing a phase ramp to the SLM. Phase ripple is the ratio of the intensity variability to the mean intensity.

7. WAVEFRONT QUALITY

Two-photon excitation has superior confinement as compared to one-photon excitation because the probability of simultaneous excitation by two photons is proportional to the square of the light intensity. Thus, two-photon excitation decays with the fourth power of distance from the focal point [8]. However, this low probability of excitation makes the mode of operation sensitive to aberrations, which alter the PSF of a focal point. To ensure consistent excitation across a large volume, it is important that the aberrations from the SLM and the remaining optics in the microscope be corrected.

Many algorithms for characterizing and correcting aberrations are based on Zernike Polynomials. However, the dependence on circular apertures is inappropriate for describing aberrations in square or rectangular arrays. Alternative strategies based on interfering sub-apertures of the SLM have been developed [9] to ensure that aberrations across the active area of the SLM can be corrected to λ/40 or better. As shown in Figure 7 the native wavefront aberrations of MLO SLMs are low due to the fabrication process used. Residual errors are removed to ensure diffraction limited foci for neuron excitation.

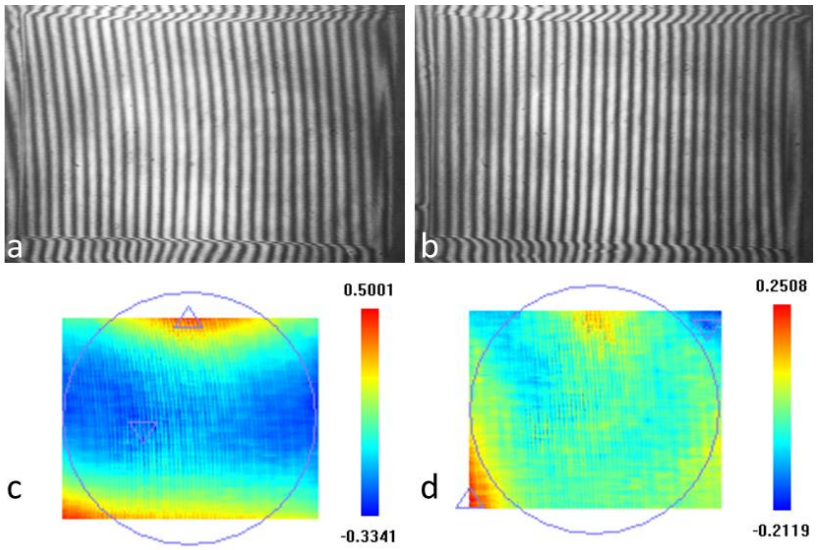

Figure. 7 (a) native wavefront of the 1920 x 1152 pixel SLM (λ/7 RMS) (b) wavefront with aberration correction applied (λ/20 RMS) (c) surface plot of aberrations without correction applied. (c) surface plot of aberrations with correction applied.

8. NEURONS PER SECOND

The goal of Optogenetics is to understand the function of neural circuits, and the relationship between firing patterns and behavior. For this to be successful, scientists need to be able to monitor and manipulate as many neurons as possible, and replicate firing patterns at rates that match that of naturally occurring circuit dynamics. There are many factors that determine how many neurons per second that can be manipulated, some of which are dependent on the experiment and others on the limits of the optical system. For example, when targeting neurons deep in the cortex, losses due to scattering are significant. The incident power cannot simply be increased to accommodate the scattering losses as there is a threshold at which laser power will cause thermal damage. In this case, limited power at the desired layer of the cortex will determine the number of neurons that can be excited. However, assuming a researcher is trying to target neurons at the same position in the cortex, specifications of the SLM will also determine the number of neurons that can be targeted per second.

There are multiple benefits to two-photon excitation for optogenetics, one of which is confinement of excitation to a depth significantly smaller than the size of a cell body. This ensures that if two neurons are directly above and below each other, excitation of the top neuron will not have sufficient power to excite the neuron below and vice versa. The problem with two-photon excitation is that the excitation confinement is so much smaller than a cell body that the focal point must be translated, or laterally expanded, to illuminate more of the cell body such that enough channels around the cell are opened to cause an action potential. Multiple strategies have been demonstrated to solve this problem. Cells can

be targeted with a single hologram, and the galvanometers can be used to spiral the illumination around the cell body. Conversely, optical strategies can be used to convert focal points into discs that spread the illumination laterally to match the width of the cell body. Either way there is an impact on the number of neurons per second that can be photoactivated. Using the spiraling approach, the focal point on the cell body is translated for about 10 ms [10]. With beam shaping, the illumination is spread, decreasing the intensity per unit area at the cell body, necessitating more power per focal point prior to beam shaping. Thus, with either strategy there is a trade between time and power.

For simplicity the spiraling method is considered in this example. The liquid crystal response time for the various SLM models is shown in Table 3. To show the impact of a slow liquid crystal switching speed, neurons per second is calculated with the standard 1920 x 1152 model, as well as with the high speed 1920 x 1152 model. Different opsins are capable of photoactivation at different rates, but for this example it is assumed that the spiral takes 10 ms. The number of groups of neurons that can be photoactivated per second is dependent on the sum of the liquid crystal response time and the spiral time. The number of neurons per group is set to 20 for the 512 x 512 pixel SLM. In this calculation it is assumed that the power per unit area incident on the SLM is held constant in the comparison of SLM models, so if the area of the SLM is increased, then the incident power can be increased such that between the different SLM models power per unit area at the SLM is constant. Increasing power over a larger area allows for a larger number of neurons to be excited per group. Thus, with the 1920 x 1152 pixel SLM the number of neurons per group is increased by the ratio of the area of the 1920 x 1152 as compared to the 512 x 512. The number of neurons that can be photoactivated per second is the number of neurons per group multiplied by the number of groups per second. Table 3 demonstrates the theoretical 1.9x increase in neurons per second that can be activated as a result of improving the SLM power handling and resolution while simultaneously maintaining the response time of the low resolution model.

Power Handling by Area Only			
Short Axis	7.68 mm	10.6 mm	10.6 mm
Area	58.98 mm^2	112.36 mm^2	112.36 mm^2
Area Ratio	1	1.9	1.9
Photoactivation Implementation			
SLM Model	ODP 512 x 512	1920 x 1152	HS 1920 x 1152
Liquid Crystal Response Time, 1064 nm	3 ms	25 ms	3 ms
Spiral Illumination on Cell Body	10 ms	10 ms	10 ms
Groups Per Second	77	29	77
Neurons Per Group	20	38	38
Neurons Per Second	1540	1102	2926

Table 3. The number of neurons that can be excited per second depends on many factors. To eliminate experimental factors, and look only at the limits of the optical system, it is assumed that 20 neurons per group can be excited. If the active area of the SLM is larger, and the power per unit area on the SLM is held constant, then the incident power can be increased which allows a larger number of neurons per group to be targeted. It is assumed that the illumination is spiraled for 10 ms per hologram such that an action potential is excited. Given the liquid crystal response time, the number of neurons per group, and the time allocated to spiraling the illumination a comparison can be made between the different SLM models of the relative number of neurons per second that can be excited.

This is clearly just a theoretical example to allow for a comparison between the different SLM models, and to see the impact to optogenetics as a result of the liquid crystal response time. Depending on the nature of the experiment, assumptions such as the number of neurons per group could be invalid but the comparative analysis would still apply.

9. CONCLUSION

Table 4 summarizes key specifications of the various SLM models and optical configurations for optogenetics, showing pixel pitch of the SLM, effective pixel pitch in the image of the SLM at the objective, the volume over which the SLM can steer focal points for excitation, the effective NA of the objective depending on how the illumination fills the back aperture, the response time of the SLM, and the number of neurons that can be excited per second. Improving the resolution of the SLM allows the beamsteering capabilities of the SLM to match the imaging capabilities of the objective without sacrificing the excitation confinement. By maintaining the response time of the SLM without using ODP, the computational load was decreased, and the number of neurons that can be excited per second increased by a

factor of 1.9. Advancing SLMs to match the capabilities of two-photon microscopes enables studies of larger neural circuits, and allows temporal dynamics of excitation at rates approaching naturally occurring circuit dynamics.

Model	Pixel Pitch	Effective Pixel Pitch	Excitation Volume	Effective NA	Response Time	Neurons Per Second
ODP 512 x 512	15 μm	18 μm	376 x 376 x 0.56 μm	1.05	3.0 ms	1540
ODP 512 x512	15 μm	9.4 μm	720 x 720 x 1.8 μm	0.55	3.0 ms	1540
1920 x 1152	9.2 μm	8.0 μm	847 x 847 x 0.93 μm	1.05	25 ms	1102
HS1920 x 1152	9.2 μm	8.0 μm	847 x 847 x 0.93 μm	1.05	3.0 ms	2926

Table 4. Summary of specifications for two-photon excitation given the various MLO SLM models highlighting the differences in excitation volume, effective numerical aperture, liquid crystal response time, and the resulting neurons that can be excited per second assuming an Olympus XLPlan N objective and an incident wavelength of 940 nm.

REFERENCES

[1] Alzheimer's Association, "Alzheimer's Disease Facts and Figures," Alzheimer's & Dementia 9 (2), 1-58 (2013).

[2] Gunaydin, L.A., Yizhar, O., Berndt, A., Sohal, V.S., Deisseroth, K., and Hegemann, P., "Ultrafast optogenetic control," Nat Neurosci. 13(3), 387-92 (2010).

[3] Nikolenko, V., Poskanzer, K., and Yuste, R., "Two-photon photostimulation and imaging of neural circuits," Nature Methods 4, 943 – 950 (2007).

[4] Nikolenko, V., Peterka, D. S, and Yuste, R., "A portable laser photostimulation and imaging microscope," J. Neural Eng. 7(4), (2010)

[5] Yang, W., Miller, J. E. K., Carrillo-Reid, L., Pnevmatikakis, E., Paninski, L., Yuste, R., and Peterka, D. S., "Simultaneous multi-plane imaging of neural circuits," Neuron, 89(2), 269-284 (2016).

[6] Thalhammer, G., Bowman, R. W., Love, G. D., Padgett, M. J., and Ritsch-Marte, M., "Speeding up liquid crystal SLMs using overdrive with phase change reduction," Optics express *21*(2), 1779-1797 (2013).

[7] Wu, S.-T., and Wu, C.-S., "High-speed liquid-crystal modulators using transient nematic effect," J. Appl. Phys. 65, 527–532 (1989).

[8] Denk, W., Strickler, J.H., and Webb, W.W., "Two-photon laser scanning fluorescence microscopy", Science 248, 73-76 (1990).

[9] Čižmár, T., Mazilu, M., and Dholakia, K. "In situ wavefront correction and its application to micromanipulation," Nature Photonics *4*(6), 388-394.(2010).

[10] Packer, A. M., Russell, L. E., Dalgleish, H. W., and Häusser, M., "Simultaneous all-optical manipulation and recording of neural circuit activity with cellular resolution in vivo," Nature methods *12*(2), 140-146. (2015).